NASA's Black Marble Multiangle Nighttime Lights Temporal Composites

Zhuosen Wang, *Member, IEEE*, Ranjay M. Shrestha,
Miguel O. Román, *Senior Member, IEEE*, and Virginia L. Kalb

***Abstract*— In addition to the daily Black Marble products (VNP46A1/A2), the recently released temporal composite products (VNP46A3/A4) are generated from daily high-quality, atmospheric, and lunar-Bidirectional Reflectance Distribution Function (BRDF) corrected, Visible Infrared Imaging Radiometer Suite (VIIRS) Day/Night Band (DNB) nighttime radiances (VNP46A2). This letter describes the algorithm of NASA's Black Marble monthly and annual (VNP46A3/A4) Nighttime Light (NTL) composites that are operationally produced for multiple view angle categories and snow conditions, along with ancillary metrics and mandatory quality assurance flags. Boxplot metrics are calculated to systematically remove outliers and minimize reliance on empirical or regional thresholds. VNP46A3/A4 products represent all nighttime conditions (i.e., moon-lit and moon-free periods), leading to an increased number of high-quality observations. To fully make use of the VIIRS DNB's wide-swath (3040 km), both VNP46A3/A4 are generated for three view zenith angle categories (near-nadir, off-nadir, and all-angles) and two different snow conditions (snow-free and snow-covered). The introduction of global multidirectional data should be of interest to the scientific and applications communities. In particular, they can enable standardized intercomparisons across NTL products and allow a greater capability to track additional dimensions of NTL change, including the intrinsic characteristics of human settlements and their infrastructure. VNP46A3/A4 products are currently made available retrospectively via NASA's Level-1 and Atmosphere Archive and Distribution System (LAADS) from the start of the Suomi-National Polar-orbiting Partnership (S-NPP) mission period (c. January 2012).**

***Index Terms*— Monthly and annual composite, multiangle, NASA's black marble, nighttime lights (NTLs).**

I. Introduction

THE Visible Infrared Imaging Radiometer Suite (VIIRS) Day/Night Band (DNB) onboard the Suomi-National Polar-orbiting Partnership (S-NPP) and NOAA-20 platforms currently measures Nighttime Light (NTL) with a 750-m at nadir spatial resolution [1]. The sensitive DNB in lowlight conditions detects nighttime phenomena that are correlated with environmental variables and human activities [2]–[11].

NASA's Black Marble NTL product suite at 15 arcsec spatial resolution has been produced from the VIIRS DNB. The daily [12] top-of-atmosphere (TOA) NTL radiance (VNP46A1), lunar- Bidirectional Reflectance Distribution Function (BRDF)- and atmospheric-corrected NTL radiance (VNP46A2), and recently released monthly (VNP46A3) and annual (VNP46A4) lunar-BRDF- and atmospheric-corrected NTL radiance composites have been publicly available from the beginning of the mission to the present.

The daily NTL product is crucial to monitor short-term changes like disaster-related power outages and restoration [7]. Additionally, monthly and annual NTL composites have been widely used for mid-and long-term dynamics such as urban development and socioeconomic changes [4], [13] with reduced data volumes and uncertainties compared to daily time series. Temporal composite NTL products mitigate the outliers and gaps related to cloud, aerosol, and data quality.

Traditionally, VIIRS monthly and annual NTL composites have relied on moon-free TOA observations, corresponding to a subset of the lunar cycle (∼29.5 days) [14]–[16]. Coesfeld *et al.* [17] indicated that local factors such as view angle, acquisition time, and atmospheric parameters are the main sources of variation in these composites. The number of observations is also limited over regions with consistent cloud coverage, affecting retrieval quality. The products are also temporally biased–in fact, "monthly" moon-free composites are often produced every other ∼15 days. In contrast, NASA's Black Marble monthly and annual NTL composites (VNP46A3/A4) are derived from all (moon-free and moon-lit) atmospherically- and lunar-BRDF-corrected Black Marble NTL (VNP46A2) and are thus temporally representative of the composite periods of interest.

To reduce the uncertainties [18], [19], VNP46A3/A4 composites are produced with multiple view angle categories and snow status along with ancillary metrics of standard deviation, the number of observations, and mandatory Quality Assurance (QA) flags. This letter introduces the VNP46A3/A4 product refinement efforts to date (c. 2021), including evaluation of product performance.

II. Data and Study Area

NASA's daily, monthly, and annual Black Marble NTL products are available from the Level-1 and Atmosphere Archive and Distribution System (LAADS) Distributed Active Archive Centers (DAACs). We selected eight globally

Manuscript received December 17, 2021; revised February 17, 2022; accepted March 31, 2022. Date of publication May 20, 2022; date of current version June 2, 2022. This work was supported by the NASA's Suomi-National Polar-orbiting Partnership (Suomi-NPP) and Joint Polar Satellite System (JPSS) Program under Grant 80NSSC22K0199. *(Corresponding author: Zhuosen Wang.)*

Zhuosen Wang is with the Earth System Science Interdisciplinary Center, University of Maryland, College Park, MD 20740 USA, and also with the Terrestrial Information Systems Laboratory, NASA Goddard Space Flight Center, Greenbelt, MD 20771 USA (e-mail: zhuosen.wang@nasa.gov).

Ranjay M. Shrestha is with Science Systems and Applications, Inc., Lanham, MD 20706 USA, and also with the Terrestrial Information Systems Laboratory, NASA Goddard Space Flight Center, Greenbelt, MD 20771 USA (e-mail: ranjay.m.shrestha@nasa.gov).

Miguel O. Román is with the Leidos Inc., Civil Group, Reston, VA 20190 USA (e-mail: Miguel.O.Roman@leidos.com).

Virginia L. Kalb is with the Terrestrial Information Systems Laboratory, NASA Goddard Space Flight Center, Greenbelt, MD 20771 USA (e-mail: virginia.l.kalb@nasa.gov).

Digital Object Identifier 10.1109/LGRS.2022.3176616

TABLE I
LOCATIONS OF CHOSEN NTL COMPOSITE SITES (ONE PIXEL OF BLACK MARBLE PRODUCT)

Sites	Location	Latitude	Longitude	Tile	Land use type
Site1	Los Angeles	34.05	-118.26	h06v05	Commercial area
Site2	Los Angeles	34.01	-118.31	h06v05	Residential area
Site3	Riverdale	36.43	-119.86	h06v05	Rural
Site4	Dubai	25.08	55.14	h23v06	Commercial area
Site5	Rome	41.90	12.48	h19v04	Commercial area
Site6	Rome	41.88	12.57	h19v04	Residential area
Site7	Rome	41.86	12.68	h19v04	Residential area
Site8	Quebec City	46.86	-71.27	h10v04	Residential area

distributed sites (Table I) to evaluate product performance. We used tile h06v05, located in the southwest USA covering a spatial area of 10°× 10°, to demonstrate the overall quality of the NTL composites.

III. METHOD

NTL uncertainties related to atmospheric and lunar irradiance have been addressed by the daily atmospheric- and lunar-BRDF-corrected NTL (VNP46A2), which serves as the primary input to VNP46A3/A4. The angular effect is one of the dominant sources of NTL uncertainty [18], [20]–[23].

The daily VNP46A2 products also correct for the reflected lunar irradiance from the surface and retain the reflected artificial light. Surface reflected artificial light is a major component of the nighttime radiance acquired by the VIIRS DNB, in addition to direct artificial light. For a given NTL source, the surface reflected light from the light source during the snow-covered period is higher than snow-free conditions due to the higher snow albedo (∼0.8 for fully snow-covered) than snow-free infrastructure (∼0.15–0.2) [18]. Therefore, VNP46A3/A4 NTL composites are produced with snow-free and snow-covered conditions separately.

A. Data Filtering

Clear sky high-quality VNP46A2 data derived from the main algorithm (QA $<$ 2) are chosen for the generation of VNP46A3/A4 composites. NTL with QA $=$ 2 represent potential outliers due to aurora, incorrect snow flag, or cloud contamination [18], and are thus excluded.

B. Temporal Composite

Further potential outliers or extreme values are excluded according to boxplot metrics [24]. The NTL observations that fall out of the range of $Q1 - 1.5 \times$ IQR and $Q3 + 1.5 \times$ IQR were filtered out from the NTL temporal composites (Fig. 1). Interquartile range (IQR) is the difference between the 75th ($Q3$) and 25th ($Q1$) percentile. Unlike the Z-score [25], the boxplot metrics method does not require normal distribution of the measurements. The composites are calculated from the mean values of the remaining observations. To remove residual background noise, the NTL composite values with radiances less than 0.5 nWcm^{-2}sr^{-1} are also set to zero. This threshold

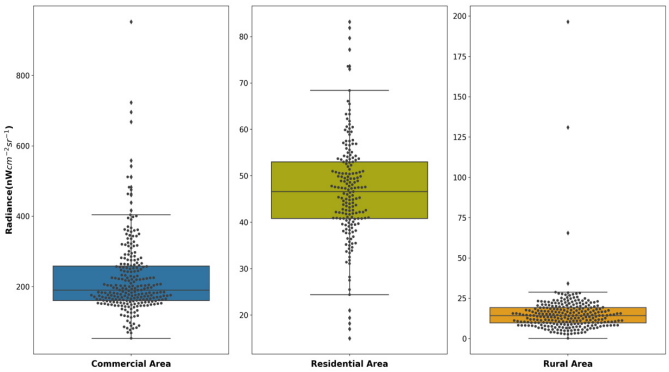

Fig. 1. Boxplot of Site 1 (commercial area), Site 2 (residential area), and Site 3 (rural area) for annual composite in 2018. The observations out of the upper and lower bars were excluded for the composite.

was obtained through a series of benchmark tests conducted using a globally stratified sample of 30 VIIRS tiles [26]. For example, we found that 5.9%, 6.0%, and 1.5% of observations were excluded for the VNP46A4 composite at the commercial (Site 1), residential (Site 2), and rural (Site 3) sites across Los Angeles in 2018, respectively (Fig. 1).

C. Output Metrics

VNP46A3/A4 NTL composites are produced at 15 arcsec spatial resolution with 28 layers including NTL radiance composite, the number of observations, QA, and NTL radiance standard deviation for three view zenith angle (VZA) categories (all-angles, near-nadir, and off-nadir) and snow conditions (snow-free and snow-covered). The boxplot outlier removal procedure was conducted for each of the angular categories and snow conditions. The VNP46 land water mask, latitude, longitude, and platform are also included as ancillary layers. The "all-angles" composite radiance is calculated based on all valid high-quality clear-sky observations. A "near-nadir" composite is also generated using the high-quality observations falling in VZA $\leq$ 20°. Finally, an "off-nadir" composite is produced from the high-quality observations with VZA $\geq$ 40°. Most of the angular information is contained in the near-nadir and off-nadir angular ranges. The all-angles composite is derived from all the angular observations, therefore, the angular composite of 20°–40° was not included in the composite products. Poor quality is assigned for the composites with a valid number of observations <4.

D. Evaluation

The chosen eight sites display conditions representative of commercial urban centers, residential, and rural areas with different snow and vegetation conditions and building heights. The coefficient of variation (CV) was utilized to evaluate the level of dispersion of the temporal Black Marble composites

$$\mathrm{CV} = \frac{\sigma}{\mu} \tag{1}$$

where σ represents the standard deviation and μ is the mean value. The CV was calculated based on all the data available for daily, monthly, and annual NTL composite from 2012 to 2021.

IV. RESULTS

For this assessment, most artificial lights at night are located between 50° and 20° latitude in the Northern

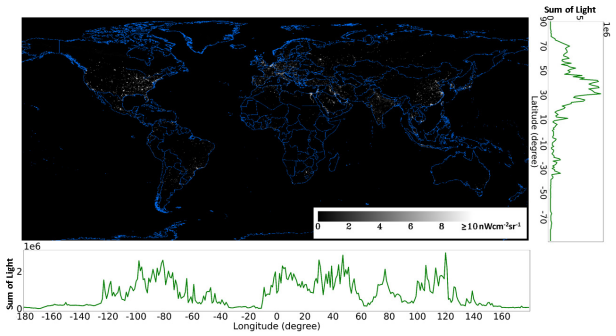

Fig. 2. Annual snow-free all-angles NTL composite in 2018. (Right) SOL radiance within each 1° of latitude. (Bottom) SOL radiance within each 1° of longitude.

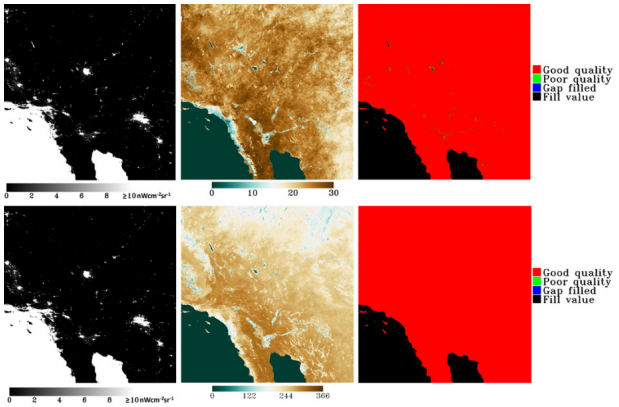

Fig. 3. Monthly in June 2016 (upper) and annual in 2016 (bottom) all-angles snow-free composite of tile h06v05 (10° × 10°). (Left) NTL composite. (Middle) Associated number of observations. (Right) QA.

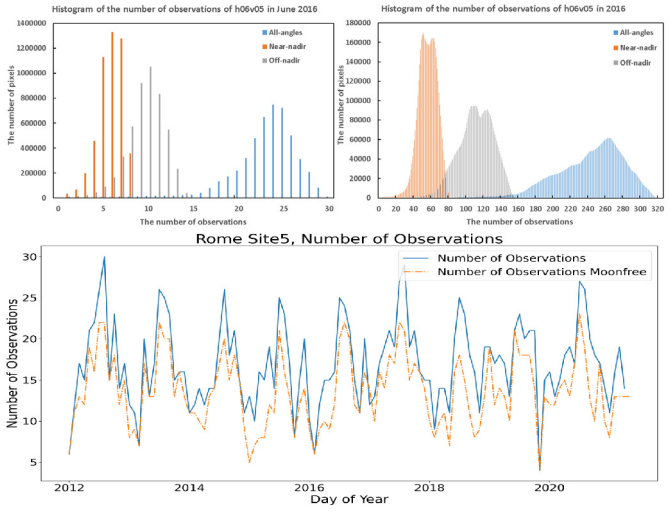

Fig. 4. Histogram of the number of valid observations for the monthly (June) (upper left) and annual (upper right) composite of tile h06v05 in 2016. And the comparison of the all valid and moon-free only number of observations for monthly composite at Site 5 (bottom).

Hemisphere (Fig. 2). Artificial lights are mainly located in the Americas, Europe, Middle East, south and East Asia.

All yearly and most areas of monthly NTL composites were flagged as good quality for tile h06v05 covering the southwest USA in 2016 (Fig. 3). The west coast around Los Angeles has relatively fewer valid observations for the temporal composite due to cloud coverage (Fig. 3). Most pixels have more than 15 observations for the monthly all-angle composite of this tile in June. For this case, VNP46A2 had 24% more valid observations than a "moon-free nights only" method employed from 2012 to 2020 at Site 5 (Fig. 4).

TABLE II
CV OF THE EIGHT SITES DURING THE SNOW-FREE PERIOD FROM 2012 TO 2021

Sites		Near-Nadir		Off-Nadir		All-Angles	
	Daily	Monthly	Annual	Monthly	Annual	Monthly	Annual
Site1	0.55	0.26	0.11	0.13	0.09	0.15	0.08
Site2	0.23	0.10	0.05	0.10	0.05	0.09	0.04
Site3	0.43	0.21	0.05	0.18	0.06	0.14	0.06
Site4	0.80	0.7	0.08	0.13	0.07	0.12	0.08
Site5	0.64	0.47	0.34	0.10	0.08	0.16	0.04
Site6	0.25	0.23	0.22	0.22	0.21	0.22	0.21
Site7	0.31	0.19	0.14	0.18	0.13	0.15	0.13
Site8	0.61	0.45	0.18	0.40	0.07	0.39	0.07

A. Temporal Comparison

As reported in recent uncertainty assessments [18], NTL radiance usually increases toward higher VZA, particularly across rural and residential regions. In contrast, NTL radiance across commercial urban centers follows a reverse trend (highest near nadir, decreasing with increased VZA). Case in point, Sites 1, 4, and 5 (corresponding to commercial urban centers) showed the largest variation compared to residential and rural areas (Table II, Fig. 5). The annual composite had the least temporal variation while daily NTL illustrates the highest temporal variation with the largest CV values.

Knowledge of seasonal variations in NTL is also crucial. For example, the monthly composite at Quebec City (Site 8) showed higher temporal variation compared to other residential sites due to the seasonal phenology effect. Site 8 was covered by deciduous trees while the vegetation status of other sites is stable throughout the year. The CV of the annual composite of Site 6 is larger than other sites particularly at off-nadir and all-angles since the radiances evidently decreased from 2016. No significant temporal changes were found over the three sites around Los Angeles (a mature urban center) during the last decade (Fig. 5).

B. Angular Categories

Multiangular NTL composites provide orthogonal information content corresponding to different urban NTL conditions. A typical example is when near-nadir composite radiance is highest with large variation over the three angular categories of VNP46A3/A4 products, e.g., Site 1 (Fig. 5). In contrast, off-nadir composites experienced the most stable temporal trends. The radiance of all-angles composites was slightly higher than off-nadir composites.

In another case, the off-nadir composite radiance of Site 2 was slightly higher than the all-angles and near-nadir composites. The near-nadir composite radiance of various commercial centers (Site 1, Site 4, and Site 5) was also much higher than the other two angular composites. The radiances of three sampled angular composites are close over the two residential sites around Rome (Site 6 and Site 7) (Fig. 6).

Additional temporal trends can be identified from different angular composites that would otherwise remain missing from composites that use single "near-nadir" or "all-angle" values. For example, near-nadir radiance spiked to high values at

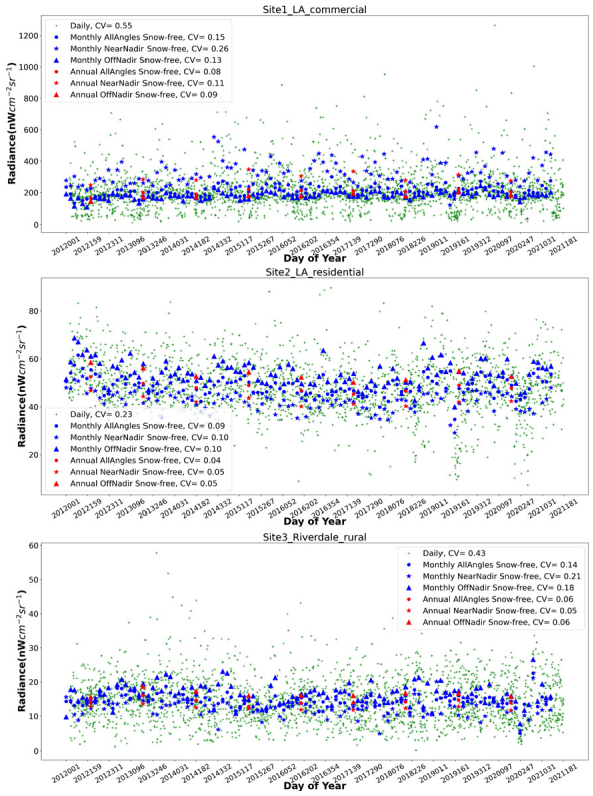

Fig. 5. Black marble daily, monthly, and annual snow-free NTL composite radiance at commercial (Site 1), residential (Site 2), and rural (Site 3) areas from 2012 to 2021.

Site 4 and Site 5 after the year 2015 which could be caused by more beam lights pointing directly at the zenith (Fig. 6). The high radiance of near-nadir composite at Dubai (Site 4) dropped to close to the other angular composites since 2020, which could be due to containment measurements associated with the COVID pandemic [27] or construction. The radiance of the two Rome residential sites (Site 6 and Site 7) decreased significantly after 2017. This particular NTL change can be attributed to the transition of yellow/orange street lights to LED by the public lighting system conventional lamps replacement project of the Municipality of Rome [28]. Fig. 6(c) illustrates this through color photographs of Rome, Italy, taken by the astronauts on the ISS in 2015 and 2021. A similar change was also found in Milan, Italy, due to the lack of light sensitivity of DNB in the range of 400–500 nm [29]. The standard deviation (the magnitude of the shaded areas in Fig. 6) is smaller after 2017 for both sites, likely due to the change of lighting types.

C. Snow

The effect of snow flag accuracy used for Collection V001 Black Marble product was discussed in Wang *et al.* [18]. The radiance of VNP46A3 during the snow-covered period is about twice as high as snow-free values at Quebec City (Fig. 7). Black Marble daily BRDF-corrected radiance (VNP46A2) only corrects the reflected lunar illumination. VNP46A2 includes surface reflected artificial light (e.g., road reflected streetlights) and the direct light from lamps (e.g., building façade lighting). The surface reflected artificial light over snow surface is much higher than snow-free condition resulting from the higher snow albedo given the same downward artificial light radiance. The change of NTL radiance depends on snow

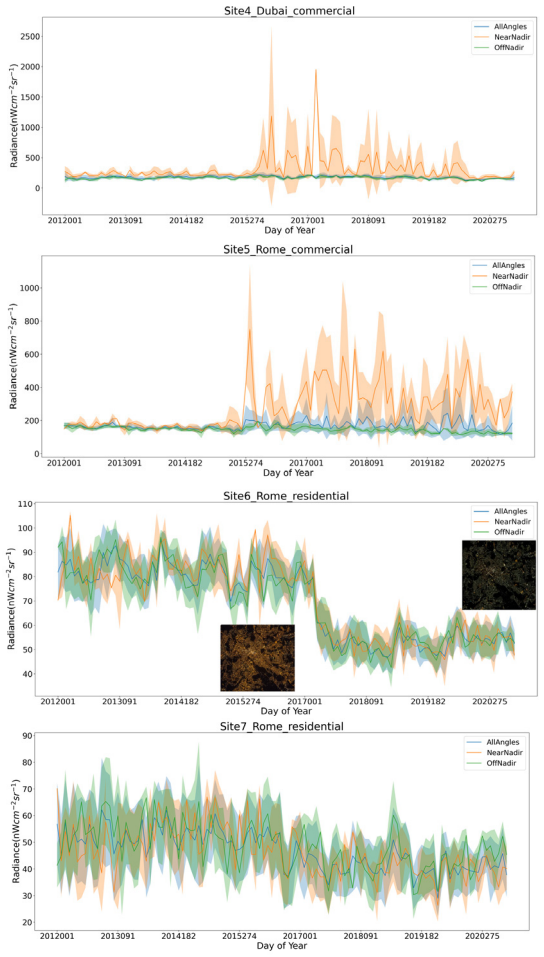

Fig. 6. Black marble temporal monthly composites at Site 4, Site 5, Site 6, and Site 7 from 2012 to 2021. The shaded areas represent the standard deviation. The International Space Station (ISS) nighttime images (https://eol.jsc.nasa.gov/) were captured in 2015 (ISS043-E-121713) and 2021 (ISS065-E-53465).

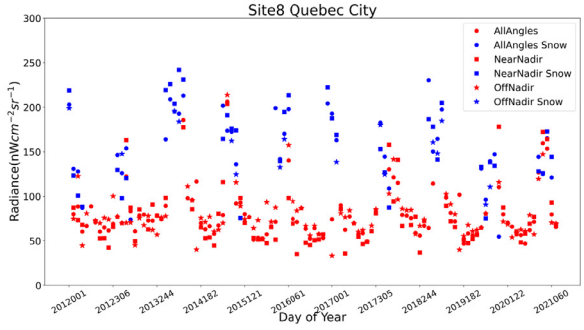

Fig. 7. Snow-free and snow-covered monthly composite radiance at Quebec City residential area (Site 8).

albedo, the proportion of surface reflected artificial light, and vegetation phenology. Vegetation occlusion is further reduced for deciduous trees during wintertime compared to the growing season since more light could penetrate the trees and be observed [30].

V. Conclusion

Black Marble monthly and annual NTL composites (VNP46A3/A4) were generated from daily lunar-BRDF-corrected NTL radiance for three view angle categories and

two snow conditions to reduce the uncertainties, along with ancillary layers providing explicit quality control. The temporal composite products have been released to the public from 2012 to the present through NASA's LAADS DAAC. Outliers were removed based on boxplot metrics and daily NTL retrieval quality. Given the use of Lunar-BRDF corrected NTLs, more high-quality observations are added into the NTL composites, helping to improve the representation of the flow of human activities over the whole period of interest, compared to approaches based on TOA moon-free nights values.

NTL composites with view angle categories significantly enhance and allow improved quantification of the detection of artificial light changes. In various instances, e.g., Dubai (Site 4) and Rome (Site 5), we show how near-nadir composite radiance increased significantly. The same response was not visible from all-angle and off-nadir NTL composites. The replacement of conventional lamps by LED street lights could also be clearly identified by multiangular composites.

As expected, the CV of monthly and annual composites is much lower than the CV of daily NTL. Our results also underpin the importance of considering the seasonal variation due to vegetation phenology and snow conditions for NTL change detection, particularly at daily and monthly scales.

We should stress that VNP46A3/A4 NTL composites labeled with "gap-filled" quality flags are populated with historical values and should not be used for quantitative analyses or change detection. Users should also be aware of the inherent flaws (background noise) when using Sum of Lights (SOLs) techniques for temporal NTL comparisons [31]. SOL is usually calculated for large areas of natural regions without artificial light. The accumulated background noise, though very low at a per-pixel level, should not be ignored when the spatial boundaries for SOL are large, especially when summarizing city- and country-scale SOL statistics.

NASA's Black Marble current product suite (Collection V001) is conservative against cloud and aurora contaminated observations; some of which may be considered as valid observations, but are nonetheless excluded by the outlier removal process. These higher-order artifacts will be mitigated further in the upcoming VIIRS Collection V002 reprocessing, which will include improved cloud masks and a newly-added Aurora QA flag using machine-learning-based detection.

REFERENCES

[1] X. Xiong *et al.*, "VIIRS on-orbit calibration methodology and performance," *J. Geophys. Res., Atmos.*, vol. 119, no. 9, pp. 5065–5078, 2014.

[2] X. Chen and W. Nordhaus, "A test of the new VIIRS lights data set: Population and economic output in Africa," *Remote Sens.*, vol. 7, no. 4, pp. 4937–4947, Apr. 2015.

[3] N. Levin *et al.*, "Remote sensing of night lights: A review and an outlook for the future," *Remote Sens. Environ.*, vol. 237, Feb. 2020, Art. no. 111443.

[4] X. Li, S. Liu, M. Jendryke, D. Li, and C. Wu, "Night-time light dynamics during the Iraqi CivilWar," *Remote Sens.*, vol. 10, no. 6, pp. 1–19, 2018.

[5] J. Wang, C. Aegerter, X. Xu, and J. J. Szykman, "Potential application of VIIRS day/night band for monitoring nighttime surface $PM_{2.5}$ air quality from space," *Atmos. Environ.*, vol. 124, pp. 55–63, Jan. 2016.

[6] W. Guo, D. Lu, Y. Wu, and J. Zhang, "Mapping impervious surface distribution with integration of SNNP VIIRS-DNB and MODIS NDVI data," *Remote Sens.*, vol. 7, no. 9, pp. 12459–12477, Sep. 2015.

[7] M. O. Román *et al.*, "Satellite-based assessment of electricity restoration efforts in Puerto Rico after Hurricane Maria," *PLoS ONE*, vol. 14, no. 6, 2019, Art. no. e0218883.

[8] M. O. Román and E. C. Stokes, "Holidays in lights: Tracking cultural patterns in demand for energy services," *Earth's Future*, vol. 3, no. 6, pp. 182–205, Jun. 2015.

[9] S. D. Miller *et al.*, "Upper atmospheric gravity wave details revealed in nightglow satellite imagery," *Proc. Nat. Acad. Sci. USA*, vol. 112, no. 49, pp. E6728–E6735, Dec. 2015.

[10] J. Wang *et al.*, "Detecting nighttime fire combustion phase by hybrid application of visible and infrared radiation from Suomi NPP VIIRS," *Remote Sens. Environ.*, vol. 237, Feb. 2020, Art. no. 111466.

[11] E. C. Stokes and K. C. Seto, "Characterizing urban infrastructural transitions for the sustainable development goals using multi-temporal land, population, and nighttime light data," *Remote Sens. Environ.*, vol. 234, Dec. 2019, Art. no. 111430.

[12] M. O. Román *et al.*, "NASA's black marble nighttime lights product suite," *Remote Sens. Environ.*, vol. 210, pp. 113–143, Jun. 2018.

[13] Q. Liu *et al.*, "Spatiotemporal patterns of COVID-19 impact on human activities and environment in mainland China using nighttime light and air quality data," *Remote Sens.*, vol. 12, no. 10, p. 1576, May 2020.

[14] Z. Zheng, Z. Wu, Y. Chen, G. Guo, Z. Yang, and F. Marinello, "A simple method for near-real-time monthly nighttime light image production," *IEEE Geosci. Remote Sens. Lett.*, vol. 19, 2021, Art. no. 8008405.

[15] Y. Hong *et al.*, "A monthly night-time light composite dataset of NOAA-20 in China: A multi-scale comparison with S-NPP," *Int. J. Remote Sens.*, vol. 42, no. 20, pp. 7931–7951, Oct. 2021.

[16] C. D. Elvidge, M. Zhizhin, T. Ghosh, F. C. Hsu, and J. Taneja, "Annual time series of global viirs nighttime lights derived from monthly averages: 2012 to 2019," *Remote Sens.*, vol. 13, no. 5, pp. 1–14, 2021.

[17] J. Coesfeld, S. Anderson, K. Baugh, C. Elvidge, H. Schernthanner, and C. Kyba, "Variation of individual location radiance in VIIRS DNB monthly composite images," *Remote Sens.*, vol. 10, no. 12, p. 1964, Dec. 2018.

[18] Z. Wang, M. O. Román, V. L. Kalb, S. D. Miller, J. Zhang, and R. M. Shrestha, "Quantifying uncertainties in nighttime light retrievals from Suomi-NPP and NOAA-20 VIIRS day/night band data," *Remote Sens. Environ.*, vol. 263, Sep. 2021, Art. no. 112557.

[19] C. C. M. Kyba *et al.*, "The benefit of multiple angle observations for visible band remote sensing using night lights," *Earth Space Sci. Open Arch. ESSOAr*, 2021, doi: 10.1002/essoar.10507575.1.

[20] X. Li *et al.*, "Anisotropic characteristic of artificial light at night—Systematic investigation with VIIRS DNB multi-temporal observations," *Remote Sens. Environ.*, vol. 233, Nov. 2019, Art. no. 111357.

[21] K. P. Tong, C. C. M. Kyba, G. Heygster, H. U. Kuechly, J. Notholt, and Z. Kolláth, "Angular distribution of upwelling artificial light in Europe as observed by Suomi–NPP satellite," *J. Quant. Spectrosc. Radiat. Transf.*, vol. 249, Jul. 2020, Art. no. 107009.

[22] C. D. Elvidge, F.-C. Hsu, M. Zhizhin, T. Ghosh, J. Taneja, and M. Bazilian, "Indicators of electric power instability from satellite observed nighttime lights," *Remote Sens.*, vol. 12, no. 19, p. 3194, Sep. 2020.

[23] X. Li *et al.*, "Using radiant intensity to characterize the anisotropy of satellite-derived city light at night," *Remote Sens. Environ.*, vol. 271, Mar. 2022, Art. no. 112920.

[24] J. Tukey, *Exploratory Data Analysis*. Boston, MA, USA: Addison-Wesley, 1977.

[25] E. Kreyszig, *Advanced Engineering Mathematics*. Hoboken, NJ, USA: Wiley, 1979.

[26] M. O. Román *et al.*, "NASA's black marble nighttime lights product suite," *Remote Sens. Environ.*, vol. 210, pp. 113–143, Jun. 2018.

[27] E. C. Stokes and M. O. Roman, "Tracking COVID-19 urban activity changes in the Middle East from nighttime lights," *Sci. Rep.*, vol. 12, no. 1, pp. 1–13, 2021, doi: 10.21203/rs.3.rs-990497/v1.

[28] D. Campisi, S. Gitto, and D. Morea, "Light emitting diodes technology in public light system of the municipality of Rome: An economic and financial analysis," *Int. J. Energy Econ. Policy*, vol. 7, no. 1, pp. 200–208, 2017.

[29] C. C. M. Kyba *et al.*, "Artificially lit surface of Earth at night increasing in radiance and extent," *Sci. Adv.*, vol. 3, no. 11, Nov. 2017, Art. no. e1701528.

[30] N. Levin and Q. Zhang, "A global analysis of factors controlling VIIRS nighttime light levels from densely populated areas," *Remote Sens. Environ.*, vol. 190, pp. 366–382, Mar. 2017.

[31] J. Coesfeld, T. Kuester, H. U. Kuechly, and C. C. M. Kyba, "Reducing variability and removing natural light from nighttime satellite imagery: A case study using the VIIRS DNB," *Sensors*, vol. 20, no. 11, p. 3287, Jun. 2020.